Near-Room-Temperature Single-Photon Emission from a Strongly Confined Piezoelectric InAs Quantum Dot

N. G. Chatzarakis,[1,2,*] S. Germanis,[3] I. Thyris,[1] C. Katsidis,[4] A. Stavrinidis,[2,4] G. Konstantinidis,[2,4] Z. Hatzopoulos,[2,4] and N. T. Pelekanos[1,2]

[1] *Department of Materials Science and Technology, University of Crete, P.O. Box 2208, 71003 Heraklion, Greece*
[2] *Microelectronics Research Group, IESL-FORTH, P.O. Box 1385, 71110 Heraklion, Greece*
[3] *College of Engineering, Mathematics and Physical Sciences, University of Exeter, Exeter, EX4 4QF, United Kingdom*
[4] *Department of Physics, University of Crete, P.O. Box 2208, 71003 Heraklion, Greece*

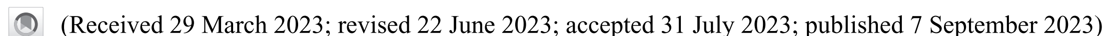

(Received 29 March 2023; revised 22 June 2023; accepted 31 July 2023; published 7 September 2023)

We demonstrate single-photon emission in strongly confined piezoelectric (211)*B* InAs/GaAs quantum dots at an elevated temperature of 230 K, exploiting the enhanced exciton-biexciton splittings in the system. This is a high temperature allowing for noncryogenic operation of a single-photon emitter based on III-arsenide quantum dots. A determining factor toward this result is the incorporation of the quantum dot layer in between GaAs/AlAs short-period superlattices, improving drastically the carrier confinement and temperature stability of the dot emission, allowing the observation of distinct exciton and biexciton emission peaks up to 260 K and single-photon emission at a high temperature.

DOI: 10.1103/PhysRevApplied.20.034011

I. INTRODUCTION

Semiconductor quantum dots (QDs) are considered ideal sources of single and entangled photons, as they can emit *efficiently* and *on demand* a single photon [1–3] or a single pair of polarization-entangled photons [4] *per excitation cycle*. Focusing, in particular, on the former devices, ultrabright single-photon emitters with high repetition rates and spectral purity have been demonstrated using epitaxial InAs QDs, exploiting the superior light-guiding properties and collection efficiencies of dot-in-wire [5], micropillar [6], and other photonic structures such as circular Bragg gratings [7,8], photonic crystal waveguides [9], and microlenses [10,11]. Importantly, the InAs QDs are able to provide single photons with a high degree of indistinguishability [6,8,10,12], a prerequisite for many quantum processing schemes. Moreover, these sources can be readily integrated into real-world devices, addressing one or more technological issues, such as deterministic positioning of QDs in the photonic structure [6–8, 10], direct coupling with fiber optics[13,14], and implementation of electrical injection schemes [15–17], taking advantage of the highly developed III-V semiconductor microfabrication technology. For practical reasons, the "on-demand" single-photon emitters should be able to emit single photons even at high temperatures. With increasing temperature, however, the InAs-based single-photon emitters rapidly lose their brightness and single-photon purity, requiring, in general, cryogenic temperatures to operate, and thus, the inconvenience of bulky and expensive cryocoolers. High temperatures reported so far for single-photon emission from InAs-based QDs are 120 K under optical excitation [18] and 77 K under electrical injection [19]. The main reasons for the temperature limitation are first, the minute exciton-biexciton (X-XX) splittings in the system, typically of a few meV [20–22], which, at elevated temperatures, undermine the single-photon purity of the exciton (X) emission by the adjacent thermally broadened biexciton (XX) line. Second, the relatively small energy difference between the energy gap of the wetting layer (WL) and the QD exciton energy, $\Delta E = E_{\mathrm{WL}} - E_{\mathrm{QD}} \cong 100$ meV, which allows for efficient thermionic emission of the QD carriers into the WL, leading to strong suppression of the emission intensity at elevated temperatures.

By comparison, single-photon emission at room temperature has been achieved in other *epitaxial* QD systems, such as GaN/(Al, Ga)N dots in wire [23], GaN/AlN QDs [24], CdSe/ZnSe dots in wire [25], and CdSe/ZnSSe/MgS QDs [26]. A common characteristic of these systems is the large X-XX splittings (20–25 meV for CdSe and 30–40 meV for GaN QDs), which are comparable to the respective exciton homogeneous linewidths at ambient temperature, enabling the QD excitons to emit single photons with sufficient purity at high temperatures. Another feature of these systems is the generally large band

*nchatz@materials.uoc.gr

 © 2023 American Physical Society

offsets and ΔE values, which are able to suppress the carrier thermionic emission from the QDs, allowing for efficient single-photon emission at elevated temperatures. Several other *nonepitaxial* systems have already been proposed in the literature as single-photon emitters at room temperature, each carrying, however, one or more disadvantages, such as single molecules of terrylene [27], suffering from photobleaching phenomena; nitrogen-vacancy color centers in artificial diamond [28,29], exhibiting long radiative lifetimes and broad emission spectra; color centers in two-dimensional hexagonal boron nitride [30], lacking control of the type and density of optically active defects; and finally colloidal CdSe QDs [31] presenting significant photoblinking, spectral diffusion effects, and long spontaneous-emission lifetimes [32,33].

Here, we revisit the technologically relevant case of InAs QDs and demonstrate that, by appropriate band-gap engineering of the QD surroundings, it is possible to obtain efficient single-photon emission up to an elevated temperature of 230 K. It should be noted that this is essentially a *noncryogenic* temperature, in the sense that it can be provided by a relatively inexpensive thermoelectric cooler [34]. Toward this end, specially designed piezoelectric (PZ) InAs QD samples are grown by molecular beam epitaxy (MBE) using the Stranski-Krastanov (S-K) growth mode on (211)*B* GaAs substrates [35]. In this orientation, the InAs-based QDs carry a strong PZ field along the growth axis, resulting in a number of interesting properties. First, these dots exhibit enhanced X-XX splitting values, in the range of 4–13 meV [36–40], which are favorable for high-temperature single-photon emission at the QD exciton level, considering that the X and XX lines can remain spectrally resolved at elevated temperatures. Second, the PZ QD excitons are characterized by reduced fine-structure splitting values [36,41], which are a prerequisite for the generation of high-fidelity entangled photons [42]. Indeed, entangled photon emission has been predicted and observed in (111)*B*-oriented InAs-based nanostructures [43,44] and dots in wires [45–47]. Another interesting aspect of the (211)*B* PZ QDs is their increased sensitivity to external electric fields due to the quadratic nature of the quantum-confined Stark effect, giving rise to enhanced Stark tunings of their X lines, suggesting the feasibility of widely tunable single-photon sources [37].

Compared to prior work, here, we resort to band-gap engineering of the surroundings of the (211)*B* QDs, to enhance their temperature stability and extend their single-photon emission characteristics as near to room temperature as possible. In a previous study on the recombination dynamics of (211)*B* InAs/GaAs QDs, it was shown that the main activation mechanism for nonradiative recombination at high temperatures was associated with electron-hole pairs escaping from the QDs to the WL [39]. This is testified by the activation energy, as determined by the Arrhenius plot of the photoluminescence (PL) intensity, which is found to be approximately equal to ΔE. The fact that the activation energy corresponds to the escape of electron-hole pairs as a whole, rather than separate electrons or holes, strongly suggests that the thermionic escape rates of electrons and holes from the QD to the WL are comparable. The above clearly indicate that, to increase the operating temperature of (211)*B* InAs QDs as single-photon emitters, we need to increase this activation energy. This can be achieved either by "pushing" the WL energy to higher energies, making use of appropriate (Al, Ga)As barriers around the QD layer, or by shifting the QD energy to lower values, increasing, for instance, the QD size up to the point of introducing dislocations and adapting to the (211)*B* orientation growth methodologies, such as the strain-relaxing layer or metamorphic buffer, which allow the emission of (100) InAs/GaAs QDs at telecom wavelengths [48,49]. In this study, we adopt the former approach, increasing the activation energy of the carriers in the QDs by encapsulating the QD layers between "digital" (Al, Ga)As alloys, issued from binary GaAs/AlAs short-period superlattices (SSLs), with different combinations of AlAs and GaAs thicknesses. In such a strongly confined piezoelectric QD system, we demonstrate single-dot emission up to 260 K, with the X and XX lines remaining resolved at all temperatures, which is not reported up to now for InAs-based QDs. As a consequence of the enhanced temperature stability in these dots, we report clear antibunching behavior at temperatures up to 230 K from single PZ QDs embedded in a microcavity.

II. SAMPLES AND EXPERIMENTAL TECHNIQUES

The strongly confined PZ InAs QD samples of this work are schematically presented in Fig. 1(a). They are grown by MBE on a (2-11)*B* GaAs semi-insulating substrate and contain a single QD layer embedded between digital (Al, Ga)As alloys, consisting of two "mirror" GaAs/AlAs SSLs, to increase carrier confinement inside the dots and the WL. The relative x and y thicknesses of the binary layers in the SSL period define the "effective" Al composition of the digital (Al, Ga)As alloy, as $\langle \mathrm{Al} \rangle = y/(x+y)$. The reason behind the use of GaAs/AlAs SSLs instead of real alloys is the moderate crystal quality of (Al, Ga)As layers obtained in the (211)*B* orientation due to growth-related difficulties related to the modified kinetics of Ga and Al adatoms on the stepped (211)*B* surface. Furthermore, the choice of digital alloys allows us to nucleate the InAs QDs always on a GaAs surface independently of the SSL's effective Al composition, ensuring reproducible QD size and density characteristics. The QD layer is grown in the S-K mode directly on the bottom SSL, by deposition of about two monolayers (MLs) of InAs at 480 °C, using either of two different growth rates of 0.1

and 0.9 ML/s. Under these conditions, the QDs take the form of truncated pyramids with typical heights between 2 and 3 nm, an aspect ratio of about 10, and a density ranging between 7×10^9 and 2×10^{10} cm^{-2}, depending on the growth rate. The above numbers are deduced by atomic-force-microscopy measurements on reference samples, where identically grown QD layers are left uncapped. Much lower QD densities of about 7×10^8 cm^{-2} can be achieved by carefully adjusting the amount of deposited InAs, just above the critical thickness for S-K growth in the (211)B orientation [35]. In most of the SSLs, the growth of the AlAs and GaAs layers occurs at the optimal growth temperature of 635 °C, with the exception of the first 10 SSL periods following the QD layer, where the growth temperature is ramped from 480 °C to 635 °C. In the studied samples, x varies between 8.6 and 23 Å, while y is kept constant at 16 Å, leading to an $\langle \text{Al} \rangle$ variation between 41% and 65%. To enhance the single-dot PL intensity by more than a decade, in addition to the above, a microcavity sample is grown, containing a strongly confined QD layer in the middle of a λ cavity, a schematic of which is given in Fig. S3 within the Supplemental Material [50]. Specifically, the λ cavity consists of a 46-period AlAs(16 Å)/GaAs(12 Å) SSL, on which the QD layer is grown, followed by a 46-period GaAs(12 Å)/AlAs(16 Å) mirror SSL. The microcavity is completed by bottom and top distributed Bragg reflectors (DBRs). The bottom DBR is a 14-period GaAs/AlAs $\lambda/4$ stack, providing a highly reflective stop band centered around 950 nm with a reflectivity higher than 99%, whereas the top DBR consists of a 4-period AlAs/GaAs $\lambda/4$ stack. The QD layer is at the antinode of the standing electromagnetic field and is grown under the conditions described above with a growth rate of 0.1 ML/s.

For the temperature-dependent macro-PL experiments, the sample is fixed on the cold finger of a variable-temperature closed-cycle helium cryostat and a He-Cd continuous-wave (cw) laser at 325 nm is employed for excitation. The PL signal is analyzed using a 0.5-m spectrograph with a 150-g/mm grating and is recorded by a liquid-nitrogen-cooled charge-coupled device (CCD) camera. To isolate the emission of single QDs, the samples are patterned by e-beam lithography into circular mesas with diameters ranging from 0.3 to 3 μm, following a layout presented elsewhere [40]. For the implementation of micro-PL (μ-PL), time-resolved PL (TRPL), and photon-correlation experiments, the patterned sample is held inside a low-vibration liquid-nitrogen-cooled cryostat, with temperatures ranging from 77 to 300 K, using a tunable Ti:sapphire laser, tuned at 750 nm, either in cw or pulsed mode of operation, with 80-MHz repetition rate and 120-fs pulse width, for excitation. The shape and size of the laser beam is adjusted by a spatial filter before entering the μ-PL setup, where it is focused on the sample by a 40× objective with numerical aperture of 0.60, giving a spatial lateral resolution of about 1.5 μm. The μ-PL signal is then collected by the same objective, analyzed by a 0.75-m spectrograph with a 1200-g/mm grating blazed at 750 nm, and recorded by a high-quantum-efficiency liquid-nitrogen-cooled back-thinned CCD. To record the photon statistics, the QD signal is directed through the side exit of the same spectrograph. The spectral window of observation is adjusted by the slit opening and can be as narrow as 50 μeV. The spectrally filtered QD signal is then split by a 50/50 nonpolarizing beam splitter in the two arms of a Hanbury Brown and Twiss (HBT) [54] setup and is collected by two fast silicon fiber-coupled single-photon avalanche photodiodes (SPADs) with 340-ps time resolution. Two mechanical irises are placed in the path before the SPADs to avoid cross-talking phenomena [55]. The photon incidences in the two detectors are time correlated using a single-photon-counting acquisition card by Becker & Hickl (SPC-130), with a channel width down to 820 fs. For the TRPL experiments of single QDs, the same acquisition card is used, utilizing the signal of one arm of the HBT setup and trigger from a fast photodiode integrated in the pulsed laser.

III. RESULTS AND DISCUSSION

The presence of the SSL barriers around the dots enhances ΔE, by affecting the WL ground state much more efficiently than the QD exciton level, due to the smaller WL thickness. This can be observed experimentally in the PL spectra of Fig. 1(b), where, by increasing $\langle \text{Al} \rangle$ from 0% to 57%, the center of weight of the QD emission bands indicated by red arrows is blueshifted by merely about 60 meV, whereas the corresponding blueshift of the WL transition shown by blue arrows is nearly 200 meV. These blueshifts can be readily accounted for, considering that an SSL with $\langle \text{Al} \rangle = 57\%$ exhibits about 0.7-eV band-gap difference at the Γ point with respect to GaAs. The indicated position of the WL transition in the reference sample at 1.415 eV is based on previous studies on similar (211)B InAs/GaAs QDs [35,39]. For the sample with $\langle \text{Al} \rangle = 41\%$, the WL peak can be distinguished as a shoulder next to the sharp GaAs substrate peaks. Notably, the intensity of the WL emission increases drastically with rising $\langle \text{Al} \rangle$. This increase cannot be ascribed to a variation in the QD density, as it does not vary significantly in these samples, but is rather attributed to enhanced carrier localization due to increasing disorder in the SSL-embedded WL, a hypothesis supported by the increased WL linewidths in the higher $\langle \text{Al} \rangle$-composition samples.

Theoretical estimates of the QD and WL transitions as a function of $\langle \text{Al} \rangle$ reproduce the experimental results reasonably well, as depicted in Fig. 1(d). The estimates, shown as solid lines, are based on the solution of a one-dimensional (1D) Schrödinger equation in the envelope-function approximation, using the NEXTNANO^3

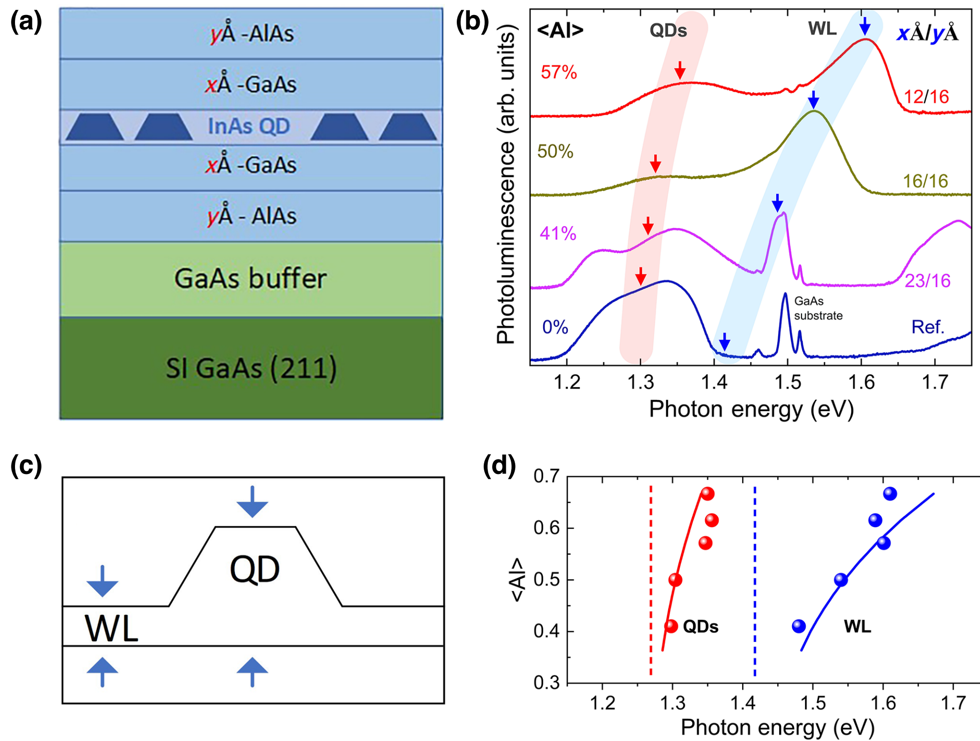

FIG. 1. (a) Schematic of the strongly confined piezoelectric InAs/GaAs QD samples, where the QD layer is embedded between GaAs/AlAs SSLs. x and y thicknesses in the SSL adjust the effective Al concentration of the digital (Al, Ga)As alloy. (b) Macro-PL spectra at $T = 20$ K of QDs embedded in GaAs(x Å)/AlAs(y Å) SSLs with different relative thicknesses of GaAs and AlAs layers, in comparison with a reference sample where the QDs are embedded in GaAs. Arrows and shaded areas mark the evolution of the QD and WL transitions with increasing Al concentration. (c) Schematic representation of a QD and corresponding WL. (d) Calculated QD and WL transition energies (solid lines) as a function of Al concentration and comparison with experimental data points. Dashed lines mark the simulated QD and WL transition energies for the reference sample.

nanostructure simulator [56]. Strain and PZ effects in the (211)B orientation are explicitly taken into account and standard III-V material parameters are used [57]. The 1D simplification is justified in our case by the large aspect ratio of the QDs, implying that quantum confinement along the growth direction is much stronger compared to the lateral direction. To take into account the intermixing effects of gallium and indium atoms, as revealed by high-resolution transmission-electron-microscopy experiments on very similar (211)B InAs/GaAs QDs [37,58], the WL and QD are considered to be $In_xGa_{1-x}As$ quantum wells of different thickness. In fact, the alloy composition and the WL and QD thicknesses are the main adjustable parameters of the simulation. Both the WL and QDs are sandwiched between two mirror GaAs/AlAs SSLs, in which the AlAs thickness is 16 Å and the GaAs thickness varies between 8 and 28 Å, translating to an ⟨Al⟩ range between 37% and 67%. The solid lines in Fig. 1(d) represent the simulated QD and WL transitions, corresponding to a particular selection of adjustable parameters, namely, an alloy of $In_{0.5}Ga_{0.5}As$, a 0.8-nm-thick WL, and a 3-nm-thick QD. With this set of parameters, the simulation reproduces rather well the data points of both transitions at high ⟨Al⟩, as well as the WL position in the reference sample (blue dashed line). On the other hand, the simulation falls a bit short on the QD position of the reference sample, which is simulated at 1.27 eV (red dashed line), instead of the value of 1.3 eV determined in Fig. 1(b). This discrepancy can be easily accounted for by a small change in the QD thickness of the reference sample. At any rate, the intention here was not to provide a precise fitting of the experimental results, but rather to reproduce their general tendency, which is that, with increasing ⟨Al⟩, the WL transition blueshifts much "faster" than the QD transition, as expected based on the smaller thickness of the WL [cf. Fig. 1(c)] and in good agreement with the experimental results.

The beneficial role of the SSL in maintaining the QD PL intensity at elevated temperatures is illustrated in Fig. 2(a), where we compare the Arrhenius plots of two QD samples, one with the SSL of ⟨Al⟩ = 65% and a reference one without the SSL. Each data point in the Arrhenius plots, corresponds to the QD PL intensity integrated over a spectral window of ±4 nm, around a wavelength of reference at a given temperature, $\lambda_{ref}(T)$. To take into account the variation of the exciton wavelength with temperature, $\lambda_{ref}(20\ K)$

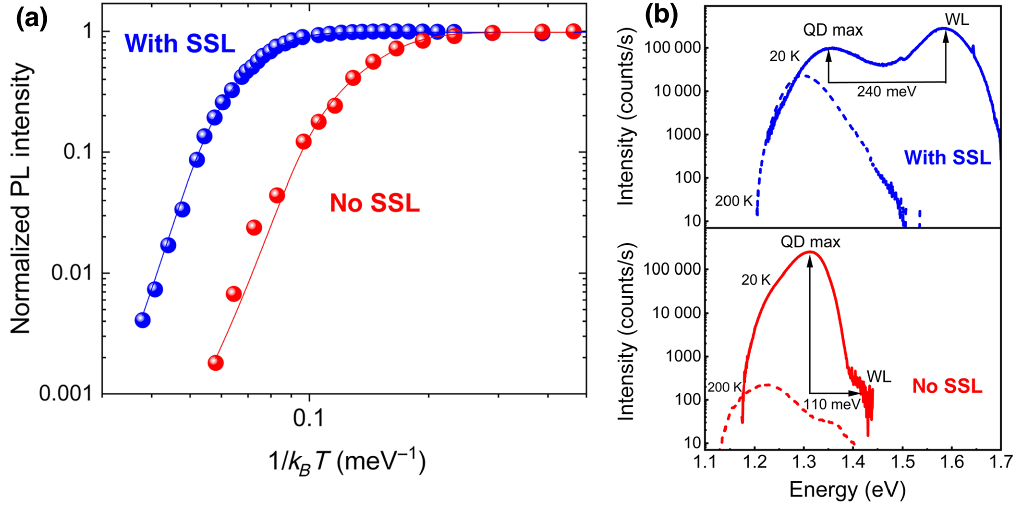

FIG. 2. (a) Arrhenius plots of normalized PL intensities for two different QD samples, with and without SSL. Solid lines are best fits of the Arrhenius equation described in the text to the corresponding data points. (b) Macro-PL spectra of the QD samples, with (upper panel) and without SSL (lower panel), at two different temperatures, highlighting the beneficial role of the SSL in maintaining the PL intensity at high temperatures. Energy difference between the QD and WL peaks is also denoted in each case.

is set at the peak of the QD emission at $T = 20$ K, while, for higher temperatures, $\lambda_{\text{ref}}(T)$ varies according to Varshni's law [59]. As shown in Fig. S1(a) within the Supplemental Material [50], the Varshni equation describing the actual temperature evolution of excitons in (211)B InAs/GaAs QDs is practically identical to that of bulk GaAs. This is partly due to the intermixing effects mentioned above, based on which the dots are in actuality three-dimensional inclusions of gallium-rich (In, Ga)As alloys [58]. Another possible reason for the dots to assimilate the character of GaAs is that a significant part of the electron wave functions extend inside the GaAs barriers, to a percentage ranging between 30% and 60%, depending on the details of the surrounding barriers, with the highest percentage corresponding to plain GaAs barriers without SSLs. By inspection of Fig. 2(a), it is clear that the PL intensity of the reference sample drops by one decade at about 120 K, while, for the sample with SSL, this occurs at the much higher temperature of about 230 K, underscoring the advantage of strong confinement for higher operating temperatures. The solid lines passing through the data points are best fits to the equation $I = I_0[1 + a\exp(-E_a/kT) + b\exp(-E_b/kT)]^{-1}$. The two exponentials correspond to different activation processes, effective in the low- and high-temperature regimes. At low temperatures, the small decrease in PL intensity observed in both samples can be accounted for by a small activation energy, $E_b \approx (35 \pm 5)$ meV, along with a weak probability coefficient, b, in the order of 100. The origin of this weak activation process is most likely exciton thermalization to the p shell of the QDs, the energy separation of which from the X line is in the order of 30 meV, as suggested by PL excitation spectroscopy. A much more efficient activation mechanism is necessary to describe the drastic drops in intensity at higher temperatures for both samples. The respective fittings to the Arrhenius equation give a much larger probability coefficient, a, in the order of 10^7, and an activation energy, E_a, of about (125 ± 15) meV for the sample without the SSL and of about (265 ± 30) meV for the sample with the SSL. As discussed earlier [39], these activation energies correspond very well to the respective ΔE values of about (110 ± 10) and (240 ± 20) meV, as indicated in the PL spectra of Fig. 2(b).

The PL enhancement at high temperatures induced by the SSLs allows us to observe single-dot emission almost at room temperature (270 K), even in samples without any microcavity-induced amplification. In Fig. 3, we show temperature-dependent μ-PL spectra from a single (211)B InAs/GaAs QD, sandwiched between GaAs(12 Å)/AlAs(16 Å) SSLs, with $\langle \text{Al} \rangle = 57\%$. The sample is processed by e-beam lithography into mesas with diameters as low as 350 nm, such as the one shown in the inset of Fig. 3. At $T = 78$ K, the μ-PL spectrum consists of two sharp lines, assigned to X and XX emissions from the same dot, based on the linear and quadratic power dependence of their intensities, respectively. In this particular dot, the XX line is blueshifted by 5.4 meV with respect to X, denoting an antibound biexciton state, something typical in PZ QDs [23,24,35–40]. By analyzing the temperature-dependent μ-PL spectra of Fig. 3, a number of useful conclusions can be reached. First of all, as illustrated in Fig. S1(a) within the Supplemental Material [50] and previously mentioned, the QD excitons redshift with temperature following the Varshni relationship for bulk GaAs rather than InAs. Second, the fact that the μ-PL signal of single QDs persists well with temperature is

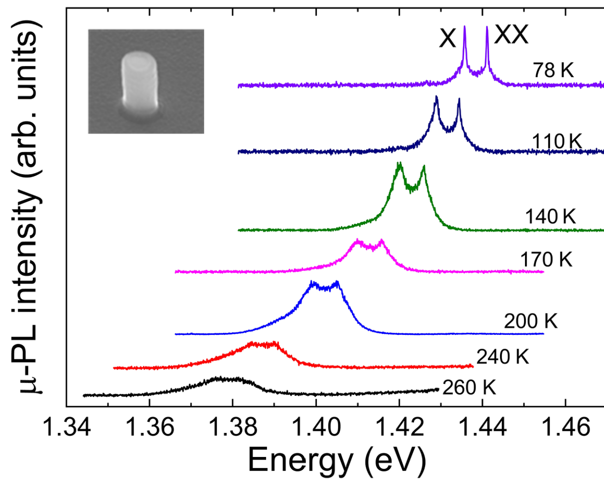

FIG. 3. Temperature-dependent μ-PL spectra of a single (211)*B* InAs/GaAs QD, which is strongly confined between GaAs/AlAs SSLs with ⟨Al⟩ = 57%. Single-dot spectra are interspaced vertically for clarity and consist of an exciton (X) and a biexciton (XX) line that remain easily resolved up to 260 K, in spite of line broadening.

a consequence of enhanced ΔE values. Specifically, the low-temperature X position of the dot in Fig. 3 is about 1.44 eV, while the WL transition energy in the same sample is about 1.61 eV [cf. top PL spectrum in Fig. 1(b)], suggesting $\Delta E \approx (170 \pm 15)$ meV for this particular dot. This ΔE value corresponds well to the activation energy of $E_a \approx (180 \pm 20)$ meV, as determined for this dot from the Arrhenius plot of Fig. S1(b) within the Supplemental Material [50]. Third, the thermal broadening of excitons in (211)*B* InAs/GaAs QDs at high temperatures is very similar to that observed in their (100) counterparts [52,60], suggesting that the high internal fields in the PZ QDs do not generate any additional broadening compared to non-PZ QDs. This is illustrated in Fig. S2 within the Supplemental Material [50], where the linewidth curves of the (211)*B* and (100) QD systems merge at $T \geq 250$ K, to full width at half maximum values of 6–7 meV. In the context of this work, the most interesting feature of Fig. 3 is clearly that the X and XX emission lines remain resolved up to 260 K. This is a prerequisite for single-photon emission with high single-photon purity at such elevated temperatures and comes as a consequence of the relatively high XX-X splittings in our system and the enhanced temperature stability of the SSL-embedded QDs.

The temperature-dependent antibunching experiments are performed on the microcavity sample, to take advantage of the approximately 1 order of magnitude enhancement of the μ-PL intensity due to the microcavity effect. In Fig. 4, we present μ-PL spectra at various temperatures from the dot that shows single-photon emission up to 230 K. For the full set of μ-PL spectra with temperature on the same dot, please refer to Fig. S4 within the Supplemental Material [50]. The excitation conditions in these spectra are identical to those used in the antibunching experiments described below. The μ-PL spectrum at 78 K contains four main peaks, marked according to their detailed assignment, as reported elsewhere [40]. With increasing temperature, the charged exciton lines (X^+ and X^-) rapidly lose intensity and at about 120 K the spectra are already mainly dominated by the X and XX emission peaks. The excitation power on the sample is

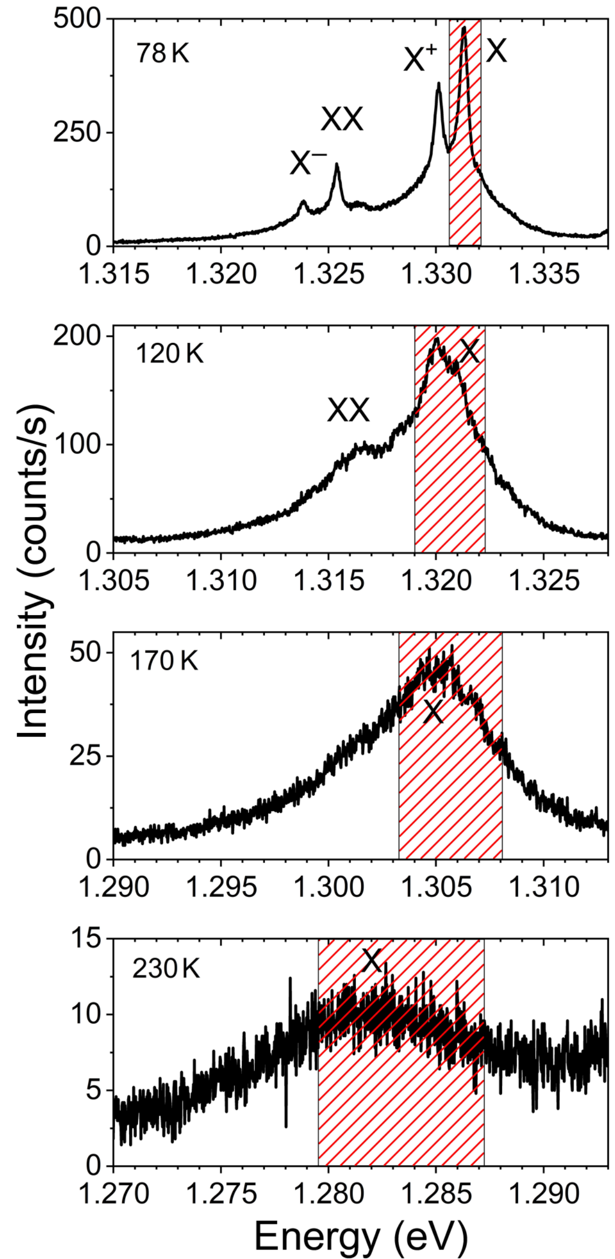

FIG. 4. Temperature-dependent μ-PL spectra under pulsed excitation from the single (211)*B* InAs/GaAs QD in a microcavity used in the antibunching experiments. Shaded areas indicate the spectral window used in the antibunching experiments at each temperature.

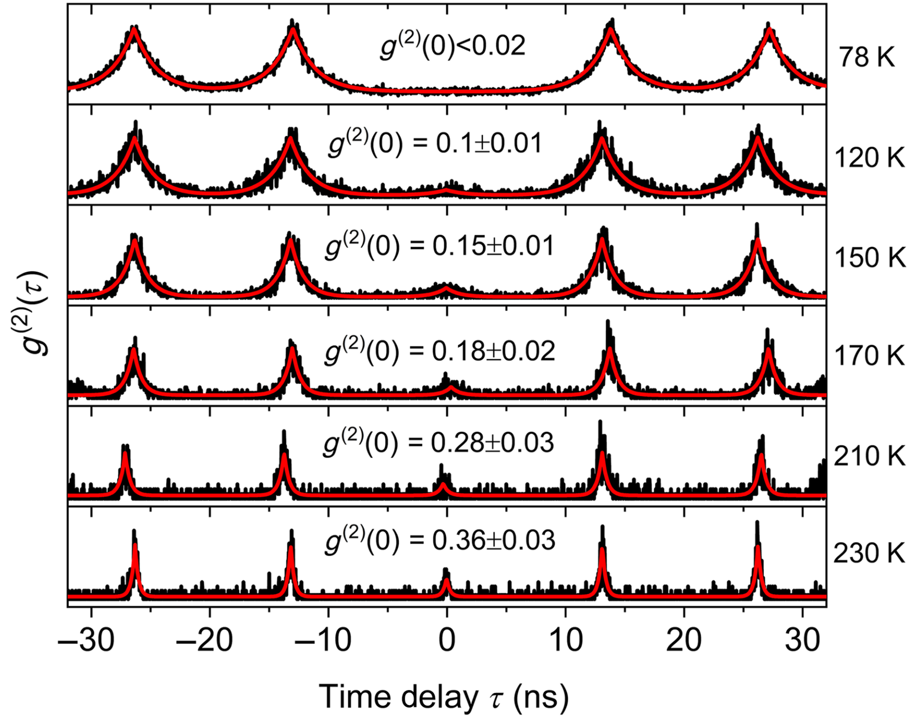

FIG. 5. Coincidence-count histograms normalized to unity obtained from 78 to 230 K using an HBT autocorrelation setup under pulsed excitation, representing the normalized second-order intensity correlation function, $g^{(2)}(\tau)$, from photons emitted at the excitonic transition of a QD.

kept constant at about 0.3 μW for all temperatures. By inspection of Fig. S5(a) within the Supplemental Material [50], this power is selected to be about a factor of 3 lower than the exciton saturation level, as a means to obtain a sufficient signal-to-noise ratio, while at the same time minimizing biexcitonic emission and ensuring high single-photon purity at the exciton level. The shaded areas in Fig. 4 indicate in each case the spectral window used in the antibunching experiment of the same temperature. It should be noted that, even if some X^+ photons coexist in the spectral window of the X emission up to some temperature, the overall single-photon characteristics should not be affected, considering that the X and X^+ lines are found to be strongly antibunched, based on cross-correlation spectroscopy [40]. In the microcavity sample, we expect enhanced temperature stability of the dots, since the QD layer is embedded between GaAs/AlAs SSLs with $\langle \mathrm{Al} \rangle = 57\%$. This is confirmed by the enhanced activation energy of $E_a = (240 \pm 20)$ meV, as determined by the corresponding Arrhenius plot shown in Fig. S5(b) within the Supplemental Material [50].

In Fig. 5, we present the normalized second-order autocorrelation function, $g^{(2)}(\tau)$, corresponding to the X line (shaded areas) of Fig. 4, obtained at various temperatures under pulsed excitation. The average photon-counting rate on each SPAD during accumulation of the coincidence histograms at 77, 120, 150, 170, 210, and 230 K was 40 000, 25 000, 16 000, 6000, 2000, and 1000 counts/s, respectively, while the respective integration times were 30, 40, 60, 120, 340, and 340 min. The dark count rate on each SPAD was about 120 counts/s. The $g^{(2)}(\tau)$ function represents the probability of detecting a coincidence photon at time τ, following the detection of a "start" photon at time zero. As expected for a single-photon emitter, the normalized $g^{(2)}(\tau)$ curves exhibit a series of intense coincidence peaks at repeat laser pulses with $\tau \neq 0$ and a "weak" or null coincidence peak around $\tau = 0$. The $g^{(2)}(0)$ values marked next to each curve are obtained by fitting the data with double exponentials, without applying any background correction, and correspond to the area under the $\tau = 0$ peak divided by that of the adjacent peaks. For all temperatures, the $g^{(2)}(0)$ values remain well below 0.5, satisfying the criterion for single-photon emission. At 78 K, in particular, $g^{(2)}(0)$ cannot be determined by fitting, due to the lack of significant coincidence counts around $\tau = 0$. Instead, we give an upper-bound estimate of $g^{(2)}(0) \leq 0.02$. Such a small $g^{(2)}(0)$ value at liquid-nitrogen temperature is not typical for a QD system. For comparison, we cite several values of $g^{(2)}(0)$ at 78 K in other systems: in optically pumped (In, Ga)As/GaAs QDs, $g^{(2)}(0)$ is between 0.177 and 0.26 [18]; in electrically pumped InAs/GaAs QDs, it is 0.35 [19]; in GaAs QDs grown by droplet epitaxy, it is 0.27 [61]; and finally in GaN/AlN QDs, it is between 0.26 and 0.35 [23]. Observing $g^{(2)}(0) \leq 0.02$ at 78 K in our case demonstrates the high single-photon purity of the (211)*B* PZ QD system, as a consequence of the large

X-XX splittings and the relatively high signal-to-background ratio at this temperature. In our system, the background photons arise mainly from emission in the WL and, to a lesser degree, in the SSL barriers of the structure. At higher temperatures, however, $g^{(2)}(0)$ increases progressively, reaching a value of 0.36 at 230 K. This is due to the relative increase of the background level with respect to the QD signal, as confirmed in the high-T spectra of Fig. 4. Another characteristic of the $g^{(2)}(\tau)$ curves is that the coincidence peaks become narrower with increasing temperature. This can be explained by the fact that the temporal profile of the coincidence peaks follows the X-decay time at a given temperature. It is worth noting that the X-decay times determined by temporal fitting of the antibunching curves are very consistent with those directly measured by us in TRPL experiments on the very same dot, as presented in Fig. S4 within the Supplemental Material [50]. To illustrate this point, in Fig. S6 within the Supplemental Material [50], we show the TRPL and antibunching curves of the same dot at 78 K, the fittings of which lead to practically the same X lifetimes.

IV. CONCLUSIONS

We have demonstrated, using a strongly confined (211)B piezoelectric InAs quantum dot, single-photon emission up to 230 K with excellent single-photon purity at liquid-nitrogen temperature. The strong confinement, provided in our case by short-period GaAs/AlAs superlattices, drastically improves the temperature stability of the dot emission by suppressing carrier escape into the wetting layer. The other key ingredient of this study is the piezoelectric orientation, which enables the large X-XX splittings in the system, and thus, the observation of spectrally resolved X and XX peaks, originating from a single quantum dot, up to 260 K. It is important to note that the above quantum dot system is capable, with minor modifications, of single-photon emission at temperatures higher than 230 K. The main parameters controlling the operating temperature are the average Al composition in the barriers, the X-XX splitting in the dot, and the position of the cavity mode. If, for example, the cavity mode in the sample of Figs. 4 and 5 were shifted to longer wavelengths by merely 50 nm, room-temperature operation would already be achievable. As a final remark, we would like to comment on the main advantage, in the context of this work, of piezoelectric quantum dot samples over conventional ones, which is that they can provide big numbers of "useful" quantum dots with sufficiently large |XX-X| splittings. In fact, in the two samples discussed in Figs. 3–5, more than 50% of the studied quantum dots showed |XX-X| larger than 5 meV.

ACKNOWLEDGMENTS

This research was supported by Greece and the European Union (European Social Fund—ESF) through the Programme "Human Resources Development, Education and Lifelong Learning 2014–2020" in the context of the project "Nanophotonic Semiconductor Sources of Single and Entangled Photons" (Grant No. MIS 5048530).

[1] P. Michler, A. Kiraz, C. Becher, W. V. Schoenfeld, P. M. Petroff, L. Zhang, E. Hu, and A. Imamoglu, A quantum dot single-photon turnstile device, Science **290**, 2282 (2000).

[2] C. Santori, M. Pelton, G. Solomon, Y. Dale, and Y. Yamamoto, Triggered Single Photons from a Quantum Dot, Phys. Rev. Lett. **86**, 1502 (2001).

[3] V. Zwiller, H. Blom, P. Jonsson, N. Panev, S. Jeppesen, T. Tsegaye, E. Goobar, M.-E. Pistol, L. Samuelson, and G. Björk, Single quantum dots emit single photons at a time: Antibunching experiments, Appl. Phys. Lett. **78**, 2476 (2001).

[4] O. Benson, C. Santori, M. Pelton, and Y. Yamamoto, Regulated and Entangled Photons from a Single Quantum Dot, Phys. Rev. Lett. **84**, 2513 (2000).

[5] J. Claudon, J. Bleuse, N. S. Malik, M. Bazin, P. Jaffrennou, N. Gregersen, C. Sauvan, P. Lalanne, and J.-M. Gérard, A highly efficient single-photon source based on a quantum dot in a photonic nanowire, Nat. Photonics **4**, 174 (2010).

[6] N. Somaschi, V. Giesz, L. De Santis, J. C. Loredo, M. P. Almeida, G. Hornecker, S. L. Portalupi, T. Grange, C. Antón, J. Demory, C. Gómez, I. Sagnes, N. D. Lanzillotti-Kimura, A. Lemaítre, A. Auffeves, A. G. White, L. Lanco, and P. Senellart, Near-optimal single-photon sources in the solid state, Nat. Photonics **10**, 340 (2016).

[7] L. Sapienza, M. Davanço, A. Badolato, and K. Srinivasan, Nanoscale optical positioning of single quantum dots for bright and pure single-photon emission, Nat. Commun. **6**, 7833 (2015).

[8] J. Liu, R. Su, Y. Wei, B. Yao, S. F, Covre da Silva, Y. Yu, J. Iles-Smith, K. Srinivasan, A. Rastelli, J. Li, and X. Wang, A solid-state source of strongly entangled photon pairs with high brightness and indistinguishability, Nat. Nanotechnol. **14**, 586 (2019).

[9] A. Laucht, S. Pütz, T. Günthner, N. Hauke, R. Saive, S. Frédérick, M. Bichler, M.-C. Amann, A. W. Holleitner, M. Kaniber, and J. J. Finley, A Waveguide-Coupled On-Chip Single-Photon Source, Phys. Rev. X **2**, 011014 (2012).

[10] M. Gschrey, A. Thoma, P. Schnauber, M. Seifried, R. Schmidt, B. Wohlfeil, L. Krüger, J.-H. Schulze, T. Heindel, S. Burger, F. Schmidt, A. Strittmatter, S. Rodt, and S. Reitzenstein, Highly indistinguishable photons from deterministic quantum-dot microlenses utilizing three-dimensional in situ electron-beam lithography, Nat. Commun. **6**, 7662 (2015).

[11] Y. Chen, M. Zopf, R. Keil, F. Ding, and O. G. Schmidt, Highly-efficient extraction of entangled photons from quantum dots using a broadband optical antenna, Nat. Commun. **9**, 2994 (2018).

[12] C. Santori, D. Fattal, J. Vuckovic, G. Solomon, and Y. Yamamoto, Indistinguishable photons from a single-photon device, Nature **419**, 594 (2002).

[13] R. S. Daveau, K. C. Balram, T. Pregnolato, J. Liu, E. H. Lee, J. D. Song, V. Verma, R. Mirin, S. W. Nam, L. Midolo, S. Stobbe, K. Srinivasan, and P. Lodahl, Efficient fiber-coupled single-photon source based on quantum dots in a photonic-crystal waveguide, Optica **4**, 178 (2017).

[14] A. Schlehahn, S. Fischbach, R. Schmidt, A. Kaganskiy, A. Strittmatter, S. Rodt, T. Heindel, and S. Reitzenstein, A stand-alone fiber-coupled single-photon source, Sci. Rep. **8**, 1340 (2018).

[15] Z. Yuan, B. E. Kardynal, R. M. Stevenson, A. J. Shields, C. J. Lobo, K. Cooper, N. S. Beattie, D. A. Ritchie, and M. Pepper, Electrically driven single-photon source, Science **295**, 102 (2002).

[16] C. L. Salter, R. M. Stevenson, I. Farrer, C. A. Nicoll, D. A. Ritchie, and A. J. Shields, An entangled light-emitting diode, Nature **465**, 594 (2010).

[17] A. Schlehahn, A. Thoma, P. Munnelly, M. Kamp, S. Höfling, T. Heindel, C. Schneider, and S. Reitzenstein, An electrically driven cavity-enhanced source of indistinguishable photons with 61% overall efficiency, APL Photonics **1**, 011301 (2016).

[18] R. P. Mirin, Photon antibunching at high temperature from a single InGaAs/GaAs quantum dot, Appl. Phys. Lett. **84**, 1260 (2004).

[19] X. M. Dou, X. Y. Chang, B. Q. Sun, Y. H. Xiong, Z. C. Niu, S. S. Huang, H. Q. Ni, Y. Du, and J. B. Xia, Single-photon-emitting diode at liquid nitrogen temperature, Appl. Phys. Lett. **93**, 101107 (2008).

[20] J. J. Finley, P. W. Fry, A. D. Ashmore, A. Lemaître, A. I. Tartakovskii, R. Oulton, D. J. Mowbray, M. S. Skolnick, M. Hopkinson, P. D. Buckle, and P. A. Maksym, Observation of multicharged excitons and biexcitons in a single InGaAs quantum dot, Phys. Rev. B **63**, 161305(R) (2001).

[21] R. M. Thompson, R. M. Stevenson, A. J. Shields, I. Farrer, C. J. Lobo, D. A. Ritchie, M. L. Leadbeater, and M. Pepper, Single-photon emission from exciton complexes in individual quantum dots, Phys. Rev. B **64**, 201302(R) (2001).

[22] S. Rodt, R. Heitz, A. Schliwa, R. L. Sellin, F. Guffarth, and D. Bimberg, Repulsive exciton-exciton interaction in quantum dots, Phys. Rev. B **68**, 035331 (2003).

[23] M. J. Holmes, K. Choi, S. Kako, M. Arita, and Y. Arakawa, Room-temperature triggered single photon emission from a III-nitride site-controlled nanowire quantum dot, Nano Lett. **14**, 982 (2014).

[24] S. Tamariz, G. Callsen, J. Stachurski, K. Shojiki, R. Butté, and N. Grandjean, Toward bright and pure single photon emitters at 300 K based on GaN quantum dots on silicon, ACS Photonics **7**, 1515 (2020).

[25] S. Bounouar, M. Elouneg-Jamroz, M. den Hertog, C. Morchutt, E. Bellet-Amalric, R. André, C. Bougerol, Y. Genuist, J.-Ph. Poizat, S. Tatarenko, and K. Kheng, Ultrafast room temperature single-photon source from nanowire-quantum dots, Nano Lett. **12**, 2977 (2012).

[26] O. Fedorych, C. Kruse, A. Ruban, D. Hommel, G. Bacher, and T. Kümmell, Room temperature single photon emission from an epitaxially grown quantum dot, Appl. Phys. Lett. **100**, 061114 (2012).

[27] B. Lounis and W. E. Moerner, Single photons on demand from a single molecule at room temperature, Nature **407**, 491 (2000).

[28] A. Gruber, A. Dräbenstedt, C. Tietz, L. Fleury, J. Wrachtrup, and C. von Borczyskowski, Scanning confocal optical microscopy and magnetic resonance on single defect centers, Science **276**, 2012 (1997).

[29] A. Beveratos, S. Kühn, R. Brouri, T. Gacoin, J.-P. Poizat, and P. Grangier, Room temperature stable single-photon source, Eur. Phys. J. D **18**, 191 (2002).

[30] T. T. Tran, K. Bray, M. J. Ford, M. Toth, and I. Aharonovich, Quantum emission from hexagonal boron nitride monolayers, Nat. Nanotechnol. **11**, 37 (2016).

[31] P. Michler, A. Imamoglu, M. D. Mason, P. J. Carson, G. F. Strouse, and S. K. Buratto, Quantum correlation among photons from a single quantum dot at room temperature, Nature **406**, 968 (2000).

[32] C. de Mello Donegá, M. Bode, and A Meijerink, Size- and temperature-dependence of exciton lifetimes in CdSe quantum dots, Phys. Rev. B **74**, 085320 (2006).

[33] O. Labeau, P. Tamarat, and B. Lounis, Temperature Dependence of the Luminescence Lifetime of Single CdSe/ZnS Quantum Dots, Phys. Rev. Lett. **90**, 257404 (2003).

[34] L. Bosco, M. Franckié, G. Scalari, M. Beck, A. Wacker, and J. Faist, Thermoelectrically cooled THz quantum cascade laser operating up to 210 K, Appl. Phys. Lett. **115**, 010601 (2019).

[35] G. E. Dialynas, S. Kalliakos, C. Xenogianni, M. Androulidaki, T. Kehagias, P. Komninou, P. G. Savvidis, Z. Hatzopoulos, and N. T. Pelekanos, Piezoelectric InAs (211)*B* quantum dots grown by molecular beam epitaxy: Structural and optical properties, J. Appl. Phys. **108**, 103525 (2010).

[36] S. Germanis, A. Beveratos, G. E. Dialynas, G. Deligeorgis, P. G. Savvidis, Z. Hatzopoulos, and N. T. Pelekanos, Piezoelectric InAs/GaAs quantum dots with reduced fine-structure splitting for the generation of entangled photons, Phys. Rev. B **86**, 035323 (2012).

[37] S. Germanis, C. Katsidis, S. Tsintzos, A. Stavrinidis, G. Konstantinidis, N. Florini, J. Kioseoglou, G. P. Dimitrakopulos, Th. Kehagias, Z. Hatzopoulos, and N. T. Pelekanos, Enhanced Stark Tuning of Single InAs (211)*B* Quantum Dots due to Nonlinear Piezoelectric Effect in Zincblende Nanostructures, Phys. Rev. Appl. **6**, 014004 (2016).

[38] G. E. Dialynas, C. Xenogianni, S. Tsintzos, E. Trichas, P. G. Savvidis, G. Constantinidis, J. Renard, B. Gayral, Z. Hatzopoulos, and N. T. Pelekanos, Anti-binding of biexcitons in (211)*B* InAs/GaAs piezoelectric quantum dots, Phys. E **40**, 2113 (2008).

[39] S. Germanis, A. Beveratos, K. Gauthron, A. Stavrinidis, G. Konstantinidis, Z. Hatzopoulos, and N. T. Pelekanos, Recombination dynamics in piezoelectric (211)*B* InAs quantum dots, Microelectron. Eng. **112**, 179 (2013).

[40] N. G. Chatzarakis, E. A. Amargianitakis, S. Germanis, A. Stavrinidis, G. Konstantinidis, Z. Hatzopoulos, and N. T. Pelekanos, Redshifted biexciton and trion lines in strongly confined (211)*B* InAs/GaAs piezoelectric quantum dots, J. Appl. Phys. **131**, 123101 (2022).

[41] J. Treu, C. Schneider, A. Huggenberger, T. Braun, S. Reitzenstein, S. Höfling, and M. Kamp, Substrate orientation dependent fine structure splitting of symmetric In(Ga)As/GaAs quantum dots, Appl. Phys. Lett. **101**, 022102 (2012).

[42] M. Larqué, I. Robert-Philip, and A. Beveratos, Bell inequalities and density matrix for polarization-entangled photons out of a two-photon cascade in a single quantum dot, Phys. Rev. A **77**, 042118 (2008).

[43] A. Schliwa, M. Winkelnkemper, A. Lochmann, E. Stock, and D. Bimberg, In(Ga)As/GaAs quantum dots grown on a (111) surface as ideal sources of entangled photon pairs, Phys. Rev. B **80**, 161307 (2009).

[44] G. Juska, E. Murray, V. Dimastrodonato, T. H. Chung, S. T. Moroni, A. Gocalinska, and E. Pelucchi, Conditions for entangled photon emission from (111)*B* site-controlled pyramidal quantum dots, J. Appl. Phys. **117**, 134302 (2015).

[45] R. Singh and G. Bester, Nanowire Quantum Dots as an Ideal Source of Entangled Photon Pairs, Phys. Rev. Lett. **103**, 063601 (2009).

[46] M. A. M. Versteegh, M. E. Reimer, K. D. Jöns, D. Dalacu, P. J. Poole, A. Gulinatti, A. Giudice, and V. Zwiller, Observation of strongly entangled photon pairs from a nanowire quantum dot, Nat. Commun. **5**, 5298 (2014).

[47] T Huber, A. Predojević, M. Khoshnegar, D. Dalacu, P. J. Poole, H. Majedi, and G. Weihs, Polarization entangled photons from quantum dots embedded in nanowires, Nano Lett. **14**, 7107 (2014).

[48] M. Paul, J. Kettler, K. Zeuner, C. Clausen, M. Jetter, and P. Michler, Metal-organic vapor-phase epitaxy-grown ultra-low density InGaAs/GaAs quantum dots exhibiting cascaded single-photon emission at 1.3 μm, Appl. Phys. Lett. **106**, 122105 (2015).

[49] M. Paul, F. Olbrich, J. Höschele, S. Schreier, J. Kettler, S. L. Portalupi, M. Jetter, and P. Michler, Single-photon emission at 1.55 μm from MOVPE-grown InAs quantum dots on InGaAs/GaAs metamorphic buffers, Appl. Phys. Lett. **111**, 033102 (2017).

[50] See the Supplemental Material at http://link.aps.org/supplemental/10.1103/PhysRevApplied.20.034011 for spectroscopy data and analysis of QD samples with and without microcavities; it includes Refs. [51–53].

[51] M. Baira, L. Bouzaiene, L. Sfaxi, H. Maaref, O. Marty, and C. Bru-Chevallier, Temperature dependence of optical properties of InAs/GaAs self-organized quantum dots, J. Appl. Phys. **105**, 094322 (2009).

[52] M. Bayer and A. Forchel, Temperature dependence of the exciton homogeneous linewidth in $In_{0.60}Ga_{0.40}As$/GaAs self-assembled quantum dots, Phys. Rev. B **65**, 041308(R) (2002).

[53] C. Kammerer, C. Voisin, G. Cassabois, C. Delalande, Ph. Roussignol, F. Klopf, J. P. Reithmaier, A. Forchel, and J. M. Gérard, Line narrowing in single semiconductor quantum dots: Toward the control of environment effects, Phys. Rev. B **66**, 041306(R) (2002).

[54] R. Hanbury Brown and R. Q. Twiss, Correlation between photons in two coherent beams of light, Nature **177**, 27 (1956).

[55] J. Bernard, L. Fleury, H. Talon, and M. Orrit, Photon bunching in the fluorescence from single molecules: A probe for intersystem crossing, J. Chem. Phys. **98**, 850 (1993).

[56] S. Birner, T. Zibold, T. Andlauer, T. Kubis, M. Sabathil, A. Trellakis, and P. Vogl, NEXTNANO: General purpose 3-D simulations, IEEE Trans. Electron Devices **54**, 2137 (2007).

[57] I. Vurgaftman, J. R. Meyer, and L. R. Ram-Mohan, Band parameters for III–V compound semiconductors and their alloys, J. Appl. Phys. **89**, 5815 (2001).

[58] N. Florini, G. P. Dimitrakopulos, J. Kioseoglou, S. Germanis, C. Katsidis, Z. Hatzopoulos, N. T. Pelekanos, and T. Kehagias, Structure, strain, and composition profiling of InAs/GaAs(211)*B* quantum dot superlattices, J. Appl. Phys. **119**, 034304 (2016).

[59] Y. P. Varshni, Temperature dependence of the energy gap in semiconductors, Physica **34**, 149 (1967).

[60] M. Benyoucef, A. Rastelli, O. G. Schmidt, S. M. Ulrich, and P. Michler, Temperature dependent optical properties of single, hierarchically self-assembled GaAs/AlGaAs quantum dots, Nanoscale Res. Lett. **1**, 172 (2006).

[61] L. Cavigli, S. Bietti, N. Accanto, S. Minari, M. Abbarchi, G. Isella, C. Frigeri, A. Vinattieri, M. Gurioli, and S. Sanguinetti, High temperature single photon emitter monolithically integrated on silicon, Appl. Phys. Lett. **100**, 231112 (2012).